Materials Science in Semiconductor Processing 63 (2017) 169–175

Contents lists available at ScienceDirect

Materials Science in Semiconductor Processing

journal homepage: www.elsevier.com/locate/mssp

Effect of sputtering power on optical properties of prepared TiO_2 thin films by thermal oxidation of sputtered Ti layers

Bandar Astinchap[a,b,*], Rostam Moradian[c], Katayon Gholami[c]

[a] Physics Department, Faculty of Science, University of Kurdistan, 66177-15175 Sanandaj, Iran
[b] Research Center for Nanotechnology, University of Kurdistan, 66177-15175 Sanandaj, Iran
[c] Physics Department, Faculty of Science, Razi University, Kermanshah, Iran

ARTICLE INFO

Keywords:
TiO_2
Thin film
RF-sputtering
Thermal oxidation
Optical properties

ABSTRACT

In this research, TiO_2 thin films prepared via thermal oxidation of Ti layers were deposited by RF-magnetron sputtering method at three different sputtering powers. The effects of sputtering power on structure, surface and optical properties of TiO_2 thin films grown on glass substrate were studied by X-ray diffraction (XRD), atomic force microscopic (AFM) and UV–visible spectrophotometer. The results reveal that, the structure of layers is changed from amorphous to crystalline at anatase phase by thermal oxidation of deposited Ti layers and rutile phase is formed when sputtering power is increased. The optical parameters: absorption coefficient, dielectric constants, extinction coefficient, refractive index, optical conductivity and dissipation factor are decreased with increase in sputtering power, but increase in optical band gap is observed. The roughness of thin films surface is affected by changes in sputtering power which is obtained by AFM images.

1. Introduction

Transparent semiconductor material (TSM) is one of the most interesting research fields, which has many applications. TiO_2, ZnO, SnO_2, In_2O_3, DLC, NiO and their compound and alloys are some of the TSM [1–5]. TiO_2 is a transparent semiconductor material with wide band gap and usually exist in three structures: rutile, anatase and amorphous [4–6]. Its thin film is widely utilized in solar cell [7], transparent electrode [8], diode [9], photocatalysts [10] and gas-sensing agents [11]. There are various methods to deposit TiO_2 thin film such as sputtering [12], sol-gel [13], dip coating and spin coating [14], filtered arc deposition [15] and laser deposition [16]. The properties of thin films strongly depend on synthesize method and deposition conditions. As reported, nucleation and growth of thin film can be controlled by deposition process and annealing temperature [17]. Therefore, choice of method and deposition condition is an important issue in studying optical properties and surface morphology of thin films. There are several reports that studied the effects of method and deposition conditions on morphology and optical properties of titania thin films. Wang et al. deposited TiO_2 thin films with Cu as impurity by DC magnetron co-sputtering and they investigated crystal texture, surface morphology, energy gap and optical properties of thin films [18]. Vyas et al. deposited TiO_2 thin films by RF magnetron sputtering and they also investigated the effect of target on structural, surface and optical properties of thin films. They found that deposited thin films with Ti target are smoother than deposited films with TiO_2 target and they also observed that the crystalline structure and band gap of deposited thin films depend on the target used [19]. The effect of gas pressure on crystalline structure, microhardness, elastic modulus, and optical properties of prepared TiO_2 thin films by reactive cathodic vacuum arc deposition has been studied by other researchers [20]. Khosravani et al. investigated structural variation of Ag-TiO_2 thin film as a function of oxidation temperature and reported that the structure of layers changed from amorphous to crystalline phase by increasing oxidation temperature [21]. Reddy et al. studied the effect of thermal annealing and oxygen partial pressure on structure and optical band gap of TiO_{2-x} films [22]. Their results revealed that the optical gap is shifted by increasing oxygen pressure. Pjević et al. reported the synthesis of TiO_2 films as a function of deposition parameters by reactive e-beam evaporation and examined the effect of annealing and substrate temperature on properties of deposited films [23,24]. Moreover, deposition of TiO_2 thin films by RF magnetron sputtering and influence of deposition parameters (RF power and sputtering pressure) on the optical properties and structure of samples were reported by Nair et al. [12]. They used TiO_2 target and sputtering power values of 100, 200 and 300 W for deposition of layers and investigated optical band gap and expression energy. In another work, Reddy et al. deposited TiO_{2-x} thin films on Si/SiO_2 wafer by RF

* Corresponding author at: Physics Department, Faculty of Science, University of Kurdistan, 66177-15175 Sanandaj, Iran.
E-mail addresses: B.astinchap@uok.ac.ir, astinchap@yahoo.com (B. Astinchap), moradian.rostam@gmail.com (R. Moradian), Gholami.katauon@gmail.com (K. Gholami).

http://dx.doi.org/10.1016/j.mssp.2017.02.007
Received 9 November 2016; Received in revised form 7 February 2017; Accepted 8 February 2017
Available online 20 February 2017
1369-8001/

reactive magnetron sputtering method and studied the effects of substrate temperatures on bolometric properties of prepared thin films [25]. They reported that rutile phase was formed in thin films structure by increasing substrate temperature and also resistivity was changed. In addition, they obtained optical band gap of TiO_{2-x} thin films which shows that optical band gap decreases with thermal annealing of thin films [26]. Recently, synthesis of TiO_2 thin films by thermal oxidation of sputtered Ti layers (obtained by DC sputtering at P = 3 kW, Ar flow=48 sccm and low pressure 10^{-3} mbar) at 600 °C for 30 min and reactive evaporation of Ti in O_2 atmosphere (5×10^{-4} mbar) were reported [27]. In this report, optical and structural properties of TiO_2 and Au/TiO_2 layers were examined and compared.

In our previous study, the influence of different deposition times on structural and optical properties of deposited TiO_2 thin films by RF magnetron sputtering was investigated [28]. However, in this work, we used Ti target and 500, 550 and 600 W values of sputtering power, and we synthesized TiO_2 thin films obtained via thermal oxidation of deposited Ti layers. The effect of sputtering power and annealing on thickness, optical properties (refractive index, extinction coefficient, optical band gap, absorption coefficient, Urbach energy, dielectric constants, optical conductivity and dispersion energy parameters) and surface morphology of layers was investigated. Multi layers thin films containing metal/semiconductor like Ti/TiO_2 are applied in electronic and optoelectronic device like fabrication of transistor and diodes [29–31].

2. Experimental

Ti layers were deposited on glass substrate by RF-magnetron sputtering (VAS models) method. Titanium layers were deposited at sputtering power of 500, 550 and 600 W for 15 min using 99.95% purity titanium target with 10 and 3 mm in diameter and thickness, respectively. Deposition was performed at room temperature and plasma formed of Ar gas (99.97% purity) in 0.2 mbar pressure was obtained. The distance between the substrate and the cathode was fixed at 10 cm. Before deposition, the glass substrates were sonicated by ethanol, acetone and double distilled water for 45 min and the chamber vacuumed to the based pressure of 5×10^{-5} mbar. To prepare the thin films of TiO_2, deposited Ti layers were annealed at different periods, where in each period, prepared thin films were annealed at 500 °C for 3 h in air. The oxidized layers (TiO_2) were formed completely for deposited Ti layers at sputtering power of 500, 550 and 600 W at periods of 2, 3 and 5 times, respectively, which are presented as T1, T2 and T3 samples (Table 1).

Crystalline structure of thin films was determined by X-ray diffractometer (STOE-STADV, Cu Kα, λ=1.54060 Å). Spectrums of UV–vis (JASCO, V-630) analysis were used to study optical parameters. And roughness was obtained by AFM (NANO SURF®) analysis.

3. Results and discussion

3.1. Structural information

The XRD patterns of the samples are shown in Fig. 1. It was observed that the sputtered titanium is formed in amorphous phase (Ti1), but after annealing processes and the formation of oxide layers, growing crystallization in anatase phase (101) has occurred (JCPDS card No. 21-127). The XRD patterns of oxide layers with different sputtering power show that by increasing sputtering power and therefore increase in thickness of oxide layer after annealing, the peak related to plane with (101) miller indices for anatase phase gets sharper and also rutile phase is formed.

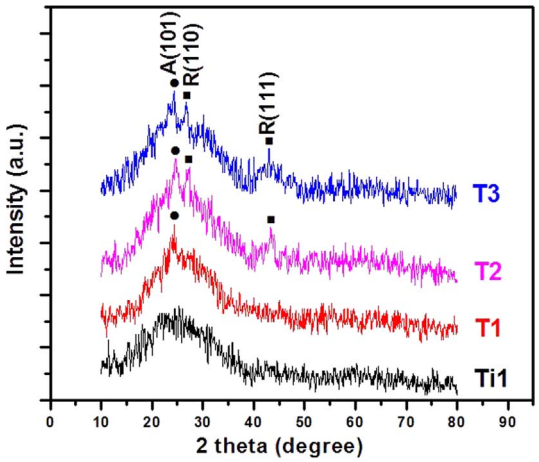

Fig. 1. The XRD patterns of prepared Ti and TiO_2 thin films by thermal oxidation of deposited Ti layer at sputtering power of 500 W (T1), 550 W (T2) and 600 W (T3).

3.2. Films morphology

Fig. 2 shows AFM images of samples' surface at the same scan area (2.02 μm^2). The images show the effect of sputtering power on morphology of deposited thin films. The roughness of thin films surface was obtained by using Mobile S software and it was shown that with increase in the sputtering power of deposition, smoother thin films grow.

3.3. Optical properties measurements

Optical transmittance spectra T(λ) of as-deposited Ti and annealed Ti thin films were measured at room temperature at wavelength range of 300–1100 nm. The optical spectra data were used to calculate optical parameters including refractive index, extinction coefficient (k), optical band gap energy (E_g^{opt}), absorption coefficient (α), Urbach tail energy (E_u), real and imaginary part of complex dielectric constants (ε_r, ε_i), dissipation factor (tan δ) and optical conductivity (σ_{opt}) for samples using Swanepoel's method [32]. In addition, thickness of thin films was obtained by using Swanepoel's formula [32] and the dispersion energy parameters were calculated from the reflective index.

3.3.1. Optical transmittance

The transmittance spectrum of Ti1 (as-deposited sample) and TiO_2 thin films (annealed Ti layers for 2 times at 500 °C) are shown in Fig. 3. It can be seen that after annealing, the thin films are transparent for wavelengths higher than 400 nm. The interference fringes are clearly observed in visible and infrared range of transmittance spectrum of samples, where the numbers of interference fringes are related to thin films thickness. Fig. 3(a) shows T(λ) for prepared layers at three

Table 1
Obtained optical parameters based on the absorption coefficients determined directly from the transmission spectra of prepared TiO_2 thin films at different sputtering powers (500 W (T1), 550 W (T2) and 600 W (T3)).

Sample	Thickness (nm)	$E_g^{opt\ (ind)}$ (eV)	$E_g^{opt\ (dir)}$ (eV)	E_o (eV)	E_d (eV)	E_u (meV)	$E_g^{opt\ (WD)}$ (eV)
T1	305 ± 0. 020	3.01	3.51	11.84	75.39	287	5.92
T2	316 ± 0. 086	3.08	3.55	5.52	27.02	270	2.76
T3	340 ± 0. 013	3.11	3.57	13.77	63.68	268	6.88

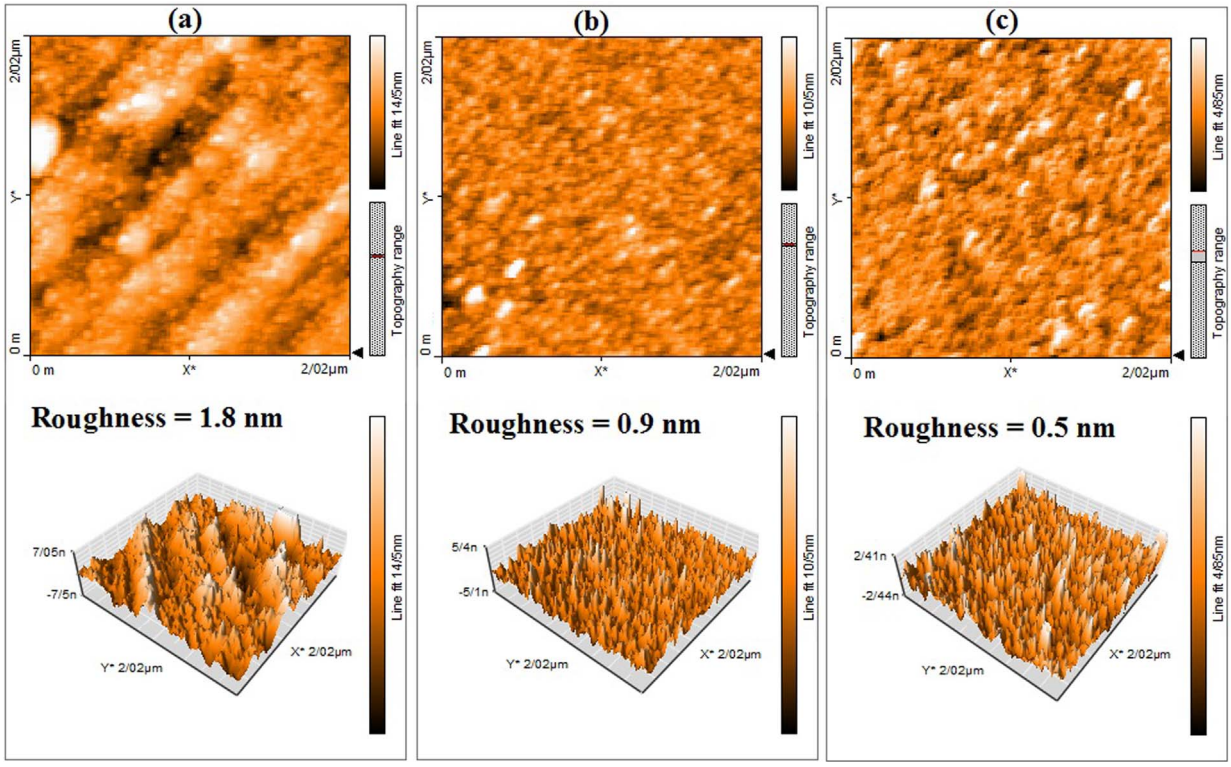

Fig. 2. Comparison of the AFM images and surface morphology of prepared thin films at three different sputtering powers (a) 500 W, (b) 550 W and (c) 600 W.

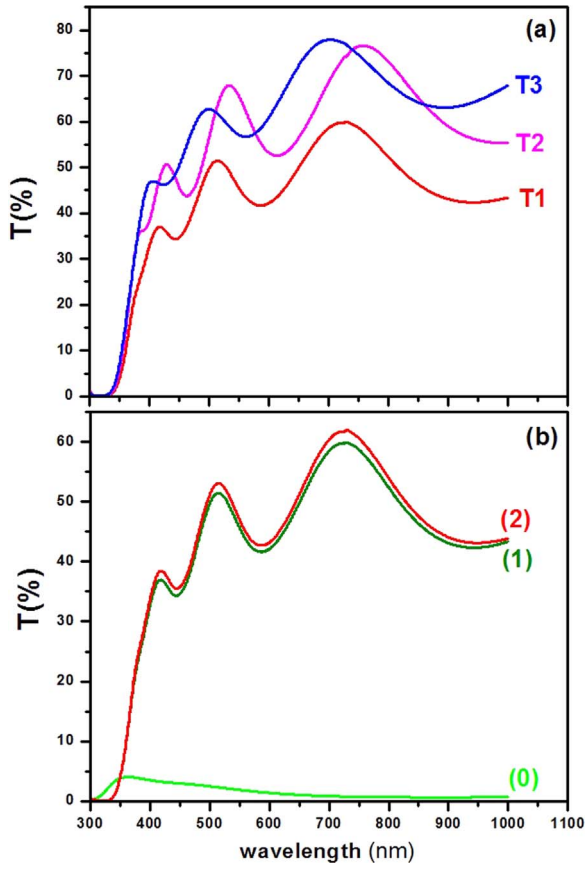

Fig. 3. (a) Transmittance spectra of prepared TiO_2 thin films by thermal oxidation of deposited Ti layers at three different sputtering powers: (T1) 500 W, (T2) 550 W and (T3) 600 W, (b) Comparison of transmittance spectra of as-deposit Ti thin film and after it's thermal oxidation at two steps.

different sputtering power (T1, T2 and T3), which indicates that transparency of layers is increased by increasing sputtering power. It can be related to the deposition of uniform layers by increasing sputtering power. The optical spectrum of sample (Ti1), prepared at 500 W sputtering powers, for as-deposited and after annealed are illustrated in Fig. 3(b). The spectrum shows that transparency of as-deposited Ti layer is close to zero, which is attributed to high absorption in metallic layer. The transparency of thin film is increased with annealing of Ti layer and the appearance of interference patterns. It is due to the change of titanium to titanium dioxide after annealing and increase in thickness of TiO_2 layer. As can be seen in Fig. 3(b), the numbers of interference fringes has not changed for annealed at Stages 1 and 2. This implies that almost all Ti layers have been converted to TiO_2 after annealing at the first stage and the resulting thickness of TiO_2 layer was constant during Stage 1 and 2. Thin film transparency was slightly increased by annealing in the second stage to the first stage, which is probably due to residual stresses removal, quantum confinement, improvement of the structure order and better oxidation of the Ti/TiO_2 film, where the last case is more probable.

3.3.2. *Films thickness, the refractive index and extinction coefficients (n, k)*

The obtained thicknesses of oxidized layer (TiO_2) for samples after annealing at air atmosphere are listed in Table 1. The thickness is calculated according to Swanepoel's method, which is based on interference pattern in transmittance spectra [32].

$$d = \frac{\lambda_1 \lambda_2}{2(\lambda_1 n_2 - \lambda_2 n_1)} \quad (1)$$

Where d is the thickness, n_1 and n_2 are the refractive indices at two adjacent maxima (or minima) at λ_1 and λ_2. The refractive indices of the films are calculated from the interference pattern in optical transmittance data using the following relationship:

$$n_\lambda = [N^2 + (N^2 - S^2)^{\frac{1}{2}} \quad]^{1/2} \quad (2)$$

where,

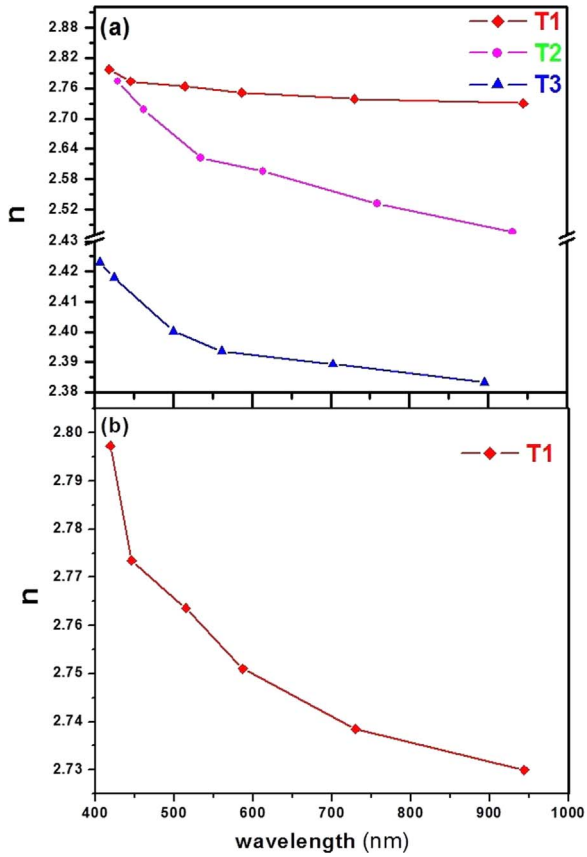

Fig. 4. (a) The refractive index for prepared samples by thermal oxidation of deposited Ti layers at three different sputtering powers: (T1) 500 W, (T2) 550 W and (T3) 600 W, (b) The refractive index for sample T1 as function of wavelength.

$$N = 2S\frac{T_M - T_m}{T_M T_m} + \frac{(S^2+1)}{2} \quad (3)$$

T_M and T_m are the tangent points in envelope function of maximum and minimum transmittance spectrum at wavelength λ, respectively. S is refractive index of glass substrate; which is 1.51.

The calculated thicknesses in Table 1 demonstrate that the thickness of deposited thin films is increased by increasing sputtering power. It can be explained by increase in plasma during sputtering by increasing sputtering power and then deposit more ions on substrate simultaneously at high power. Figs. 4 and 5 illustrate the refractive index and extinction coefficient for prepared TiO_2 thin films, which are calculated based on Swanepoel's method using transmittance spectra [32].

As shown in Fig. 4, the refractive index for prepared samples (T1, T2 and T3) has been decreased by increasing sputtering power of deposition process. Therefore, the refractive index for samples are obtained for all range of wavelength as $n_{T1} > n_{T2} > n_{T3}$. In fact, thicker TiO_2 thin films have lower refractive index as reported in our previous study [28]. This behavior may be attributed to increase in surface roughness and vacancies by increasing thickness of layers. As shown in Fig. 4, the refractive index decreases with increase in wavelength for all prepared thin films, which show normal dispersion behavior and is in line with our results of previous study and other reports [24,28,33].

The extinction coefficient (k) is an important parameter to determine some optical properties, where its values show the fraction of light loss because of scattering and adsorption per unit distance of the penetration medium. The value of extinction coefficient can be calculated as follows [32]:

$$K = (\alpha\lambda/4\pi) \quad (4)$$

where λ is wavelength and α is the absorption coefficient.

The extinction coefficients of samples (T1, T2 and T3) as function of wavelength are presented in Fig. 5. The values obtained show that k was decreased with sputtering power. Actually, the k in thinner films is higher and it can be attributed to surface roughness. As shown in Fig. 5, the variation slope of extinction coefficient is changed sharply in near ultra violet region. It is due to near absorption edge and electron transition from valence to conduction band in TiO_2 thin films.

3.3.3. Absorption coefficient and optical band gap

The absorption coefficient curves versus photon energy are shown in Fig. 6, which is investigated for oxidized layers. The absorption coefficient α was calculated using Eq. [24]:

$$\alpha = \frac{1}{d}\ln\left(\frac{1}{T}\right) \quad (5)$$

where d is film thickness and T is transmittance.

It is understood from Fig. 6 that, when sputtering power increased, there is decreased in absorption. This is in line with results of extinction coefficient (k) and transmittance spectrum (T). In fact increasing sputtering power causes more uniform surface and this leads to decrease in scattering and absorption.

It can be observed that absorption coefficient increases with increase in photon energy and absorption edge of TiO_2 thin films is shifted to the high photon energy with increase in sputtering power.

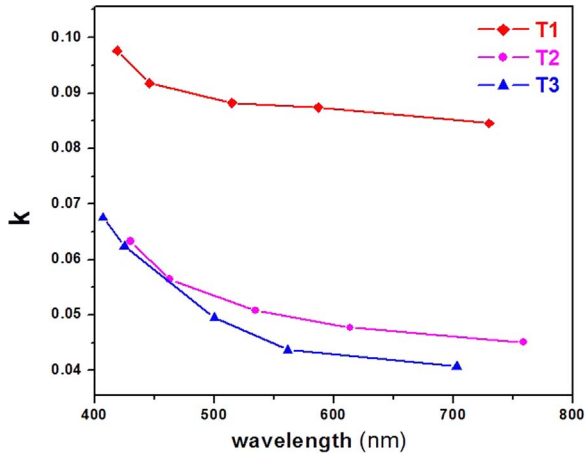

Fig. 5. The extinction coefficients for prepared samples by thermal oxidation of deposited Ti layers at three different sputtering powers: (T1) 500 W, (T2) 550 W and (T3) 600 W as function of wavelength.

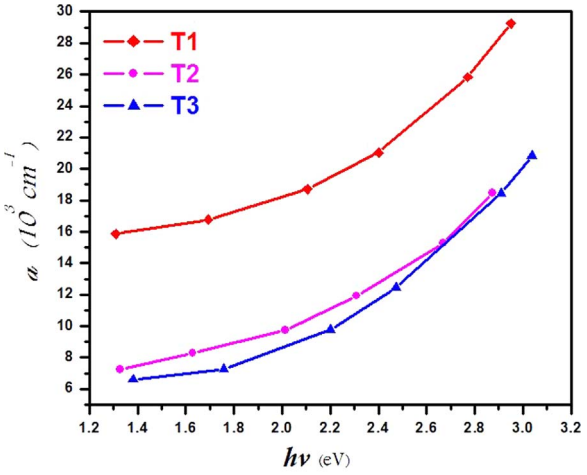

Fig. 6. The absorption coefficient curves versus photon energy for prepared TiO_2 thin films via thermal oxidation of deposited Ti layers at sputtering powers of (T1) 500 W, (T2) 550 W and (T3) 600 W.

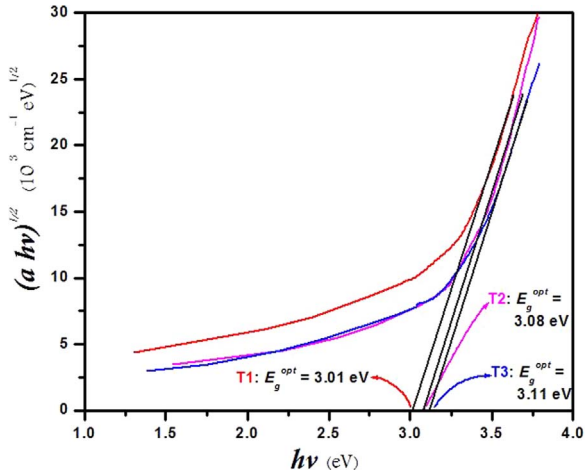

Fig. 7. Indirect optical band gap of prepared TiO_2 thin films by thermal oxidation of Ti layers deposited at sputtering powers of (T1) 500 W, (T2) 550 W and (T3) 600 W. The results show increase of indirect band gap in thicker thin films.

The absorption edge is a method of understanding electronic inter-band transitions, which occurred at UV wavelength region for TiO_2.

The optical band gap for semiconductor materials can be determined through the relationship between absorption coefficient and photon energy. Tauc's relationship is employed to calculate optical band gap in most articles and in this study, we also used it to calculate optical band gap of prepared TiO_2 thin films [35].

$$\alpha h\nu = canst\,(h\nu - E_g^{opt})^m \tag{6}$$

where $(h\nu)$ is the photon's energy and m determines transition type, which is m=1/2 for direct transition and 2 for indirect transition.

The relationship of $(ahv)^{1/2}$ and $(ahv)^2$ versus $h\nu$ for TiO_2 thin films are shown in Figs. 7 and 8, respectively. The indirect and direct optical band gaps of samples were determined by extrapolating the linear part of the plots on the $h\nu$ axis. The obtained values for indirect and direct optical band gaps are listed in Table 1. The results show that increased sputtering power has led to increase optical band gap.

3.3.4. The Urbach energy

In the low photon energy range, where the absorption spectra are dependent on the absorption edge and photon energy, the absorption coefficient curve has an exponential part which is called Urbach tail. Urbach tail due to localized states is extended in the band gap and appears in the disordered, amorphous, poor crystalline and low crystalline material [36,37]. Urbach tail energy can be determined by

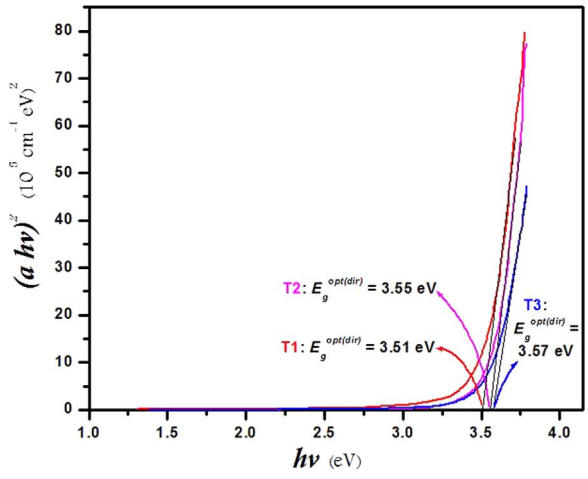

Fig. 8. Direct optical band gap of prepared TiO_2 thin films by thermal oxidation of Ti layers deposited at sputtering powers of (T1) 500 W, (T2) 550 W and (T3) 600 W.

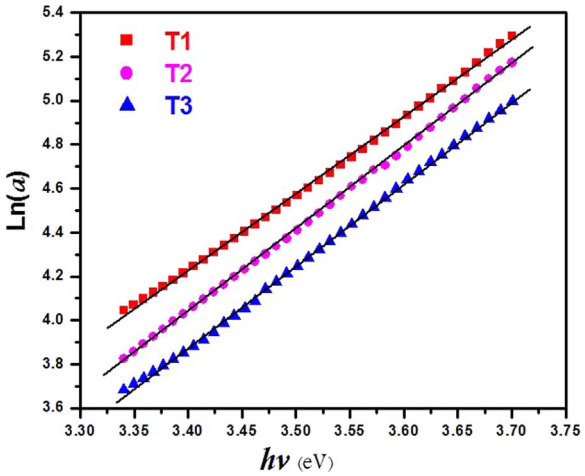

Fig. 9. The variation of Lnα with photon energy to obtain Urbach energy from the slope of curves for prepared samples at sputtering power of 500 W (T1), 550 W (T2) and 600 W (T3).

the exponential equation as follows [38]:

$$\alpha = \alpha_0 e^{\frac{h\nu}{E_u}} \tag{7}$$

$$ln\alpha = ln\alpha_0 + \left(\frac{h\nu}{E_U}\right) \tag{8}$$

where α_0 is a constant and E_u is Urbach energy (the band tail width), and it weakly depends on temperature and strongly on structural disorder.

The variation of Lnα with photon energy is shown in Fig. 9 and Urbach energy is obtained from the slope of the straight line of plotting Lnα versus photon energy. The values of E_U are listed in Table 1. It is observed that Urbach energy decrease by increasing sputtering power resulting in increase in TiO_2 film thickness. This behavior of E_U can be attributed to more annealing steps and high sputtering power which decreases defects in the structural bonding. Data obtained show that the behavior of Urbach tail is in contrast to optical band gap as reported in our previous study [28]. As can be seen from Table 1, the E_U values for samples are in range of amorphous materials as reported by N. Mott and E. Davis [39]. This confirmed the XRD results that referred to weak crystalline phases.

3.3.5. The dielectric constants (ε_r, ε_i)

The complex refractive index (N=n+ik) and complex dielectric constant (ε= ε_r+$i\varepsilon_i$) describe fundamental intrinsic optical properties of thin films. The real and imaginary parts of dielectric constant as a function of photon energy for prepared TiO_2 thin films are illustrated in Fig. 10. These parameters are determined by the following relations:

$$\varepsilon_r = n^2 - k^2 \tag{9}$$

$$\varepsilon_i = 2nk \tag{10}$$

where n and k are the refractive index and the extinction coefficient, respectively. It is observed that both the real and imaginary parts of dielectric constants decrease with increasing sputtering power, which is in line with the variation of the refractive index and the extinction coefficient. Moreover, the dielectric constant increases with photon's energy, which declares normal dispersion in the region. As shown in Fig. 10, the values of real part of dielectric constant are higher than the imaginary parts for all samples.

Dissipation factor for the prepared TiO_2 thin films at different sputtering power versus incident light frequency is shown in Fig. 11. Dissipation factor can be calculated using the following equations [4]:

$$tan\delta = \frac{\varepsilon_i}{\varepsilon_r} \tag{11}$$

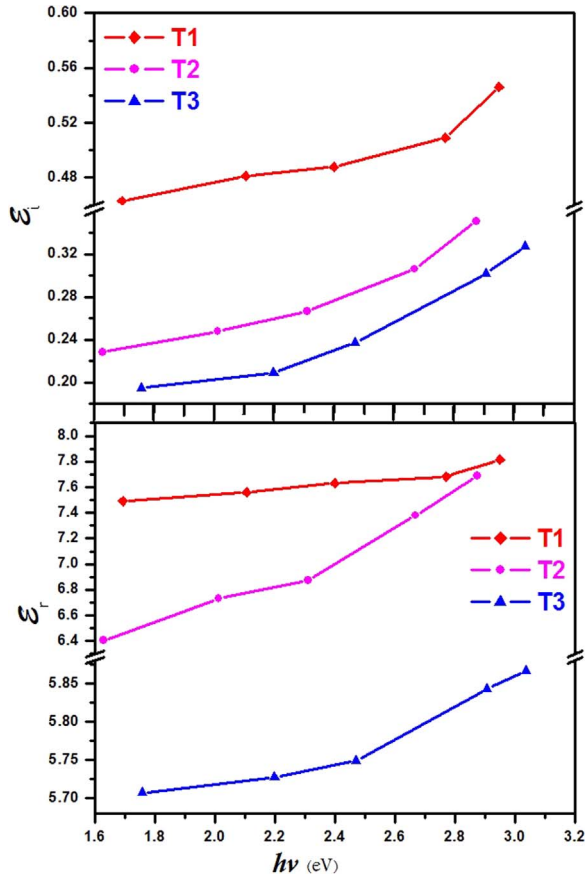

Fig. 10. The variation of the real and imaginary part of the dielectric constant with photon energy for deposited Ti layers at sputtering power of 500 W (T1), 550 W (T2) and 600 W (T3) after thermal oxidation.

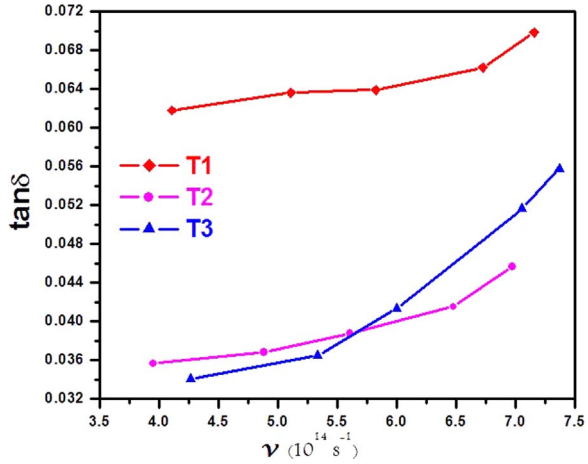

Fig. 11. Dissipation factor versus incident light frequency for prepared TiO_2 thin films at different sputtering power: 500 W (T1), 550 W (T2) and 600 W (T3).

It was found that the dissipation factor decreases by increasing sputtering power and increases with increase in photon frequencies for TiO_2 thin films. It can be related to density of thin films and surface morphology.

3.3.6. Optical conductivity

The optical conductivity (σ_{opt}) can be calculated using absorption coefficient (α) as follows [4,40]:

$$\sigma_{opt} = \frac{\alpha n c}{4\pi} \quad (12)$$

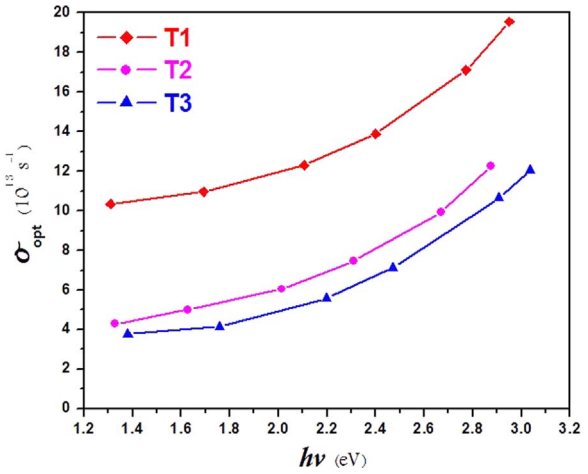

Fig. 12. The variation of obtained optical conductivity from absorption coefficient and refractive index for deposited TiO_2 thin films at different sputtering powers (500 W (T1), 550 W (T2) and 600 W (T3)).

where n is the refractive index and c is the velocity of light. The variation of optical conductivity for deposited TiO_2 thin films at different sputtering power is illustrated in Fig. 12. The σ_{opt} decreases with increasing power of sputtering, which is due to decrease in absorption. Increasing optical conductivity at high photon energy, near UV region, is due to high absorbance of TiO_2 thin films resulting in increase in electron density in conduction band [4,41].

3.3.7. Dispersion energy parameters

Didomenico and Wemple introduced single oscillator energy (E_O) and dispersion energy (E_d), based on the single-oscillator model [42,43]. The dispersion energy (E_d) measures the average oscillator strength of inter-band optical transition and explains the dispersion of the refractive index. The single oscillator energy (E_O) is the energy of the effective dispersion oscillator which has little information about the band structure of the material and it corresponds to the distance between the centers of mass of the valence and conduction bands. E_O and E_d are given from the semi-empirical dispersion relationships as follows [4–44]:

$$n^2-1 = \frac{E_d E_0}{E_0^2 - (h\nu)^2} \quad (13)$$

where n is the refractive index. These parameters can be calculated by plotting $(n^2-1)^{-1}$against $(h\nu)^2$ and fitting a straight line $(E_O\, E_d)^{-1}$ and the intercept (E_0/E_d). These are shown in Fig. 13. The values of dispersion energy parameters are shown in Table 1. The oscillator energy E_O is associated with the optical band gap, approximation by $E_g^{opt(WD)} \approx E_O/2$ [44,45]. The calculated optical band gap from absorption edge differs with $E_g^{opt(WD)}$; which is due to the investigation into range of wavelength [4]. $E_g^{opt(WD)}$ is determined in the transparent region while, E_g^{opt} is obtained in absorption region.

4. Conclusion

In this study, we have been able to synthesize Ti/TiO_2 thin films through thermal oxidation of deposited Ti layers by RF-magnetron sputtering method at 500 °C in normal atmosphere. The influence of sputtering power (500, 550 and 600) on structure, optical properties and surface morphology was investigated. From the XRD results obtained, since as-deposited Ti layers are amorphous, the crystalline structure was formed after annealing which results in the formation of TiO_2 thin films. The crystal structure of titanium dioxide layers was in anatase phase and rutile phase appeared with increase in sputtering power. Therefore, the phase of thin films is not only dependent on thermal oxidation, but also on sputtering power of deposition.

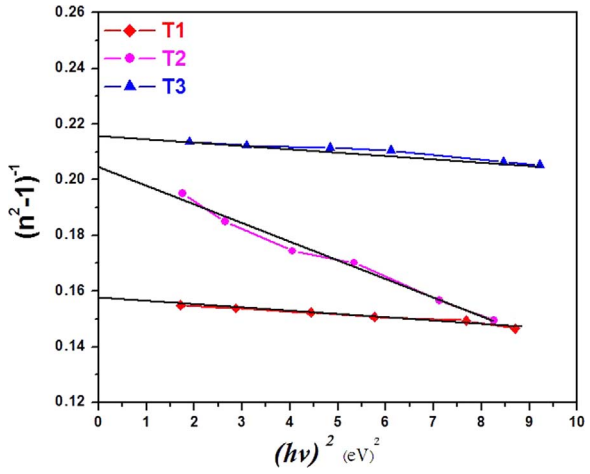

Fig. 13. Plot of the refractive index factor $(n^2-1)^{-1}$ versus $(hv)^2$ to obtain single oscillator energy (E_o) and dispersion energy (E_d) for prepared TiO_2 thin films at different sputtering powers (500 W (T1), 550 W (T2) and 600 W (T3)).

Increased sputtering power led to smoother growth (Ra_{T1}=1.8, Ra_{T2}=0.9 and Ra_{T3}=0.5) and thicker thin films, which indicated increase in plasma flux and then uniform deposition of Ti ions on the surface. The optical parameter containing: E_g, n, k, E_u, α, ε_i, ε_r and σ were obtained and studied. The results reveal that all optical parameters (E_u, α, ε_i, ε_r and σ) decreased with increasing sputtering power, but the optical band gap increased, such that its value change from 3.01 to 3.11. Therefore, the nonlinear optical parameters and crystalline structure of TiO_2 layers strongly depends on the used sputtering power.

Ultimately, it should be noted that these results could be useful for researcher and industrialists in designing of device that are based on metal/semiconductor layers, such as solar cell and diodes.

Appendix A. Supplementary material

Supplementary data associated with this article can be found in the online version at doi:10.1016/j.mssp.2017.02.007.

References

[1] B. Astinchap, R. Moradian, M. Nasseri Tekyeh, Opt.-Int. J. Light Electron Opt. 127 (20) (2016) 9871–9877.
[2] S. Abdolghaderi, B. Astinchap, A. Shafiekhani, J. Mater. Sci.: Mater. Electron. 27 (2016) 6713–6720.
[3] S. Mansouri Majd, A. Salimi, B. Astinchap, Biosens. Bioelectron. (2016). http://dx.doi.org/10.1016/j.bios.2016.09.097.
[4] M.M. Abdel-Aziz, I.S. Yahia, L.A. Wahab, M. Fadel, M.A. Afifi, Appl. Surf. Sci. 252 (2006) 8163–8170.
[5] D.A.H. Hanaor, C.C. Sorrell, J. Mater. Sci. 46 (2011) 855–874.
[6] Ch Ho Heo, S.-B. Lee, J.-H. Boo, Thin Solid Films 475 (2005) 183–188.
[7] B. O'Regan, M. Grätzeli, Nature 353 (1991) 737–740.
[8] S. Huang, T.-D. Kim, J. Luo, Steven K. Hau, Z. Shi, et al., Appl. Phys. Lett. 96 (2010) 243311.
[9] J.-J. Huang, Ch-W. Kuo, W.-Ch Chang, T.-H. Hou, Appl. Phys. Lett. 96 (2010) 262901.
[10] M. Maicu, D. Glöß, P. Frach, D. Hecker, G. Gerlach, J.M. Córdoba, J. Nanosci. Nanotechnol. 15 (9) (2015) 6478–6486.
[11] Ch Wang, L. Yin, L. Zhang, Y. Qi, N. Lun, N. Liu, Langmuir 26 (15) (2010) 12841–12848.
[12] P.B. Nair, V.B. Justinvictor, G.P. Daniel, K. Joy, V. Ramakrishnan, P.V. Thomas, Appl. Surf. Sci. 257 (2011) 10869–10875.
[13] J. Yu, X. Zhao, J. Du, W. Chen, J. Sol.-Gel Sci. Technol. 17 (2) (2000) 163–171.
[14] S.M. Jlassi, M. Hajji, M.F. Boujmil, R. Jerbi, M. Kandyla, M. Kompitsas, H. Ezzaouia, J. Sol.-Gel Sci. Technol. 72 (2014) 421–427.
[15] A. Bendavid, P.J. Martin, E.W. Preston, Thin Solid Films 517 (2008) 494–499.
[16] A. Ishii, Y. Nakamura, I. Oikawa, A. Kamegawa, H. Takamura, Appl. Surf. Sci. 347 (2015) 528–534.
[17] P. Lobl, M. Huppertz, D. Mergel, Thin Solid Films 251 (1994) 72–79.
[18] H. Wang, Y. Li, X. Ba, L. Huang, Y. Yu, Appl. Surf. Sci. 345 (2015) 49–56.
[19] S. Vyas, R. Tiwary, K. Shubham, P. Chakrabarti, Superlattices Microstruct. 80 (2015) 215–221.
[20] H. Takikawa, T. Matsui, T. Sakakibara, A. Bendavid, Ph.J. Martin, Thin Solid Films 348 (1999) 145–151.
[21] Sh Khosravani, S. Bagheri Dehaghi, M. Bagher Askari, M. Khodadadi, Microelectron. Eng. 163 (2016) 67–77.
[22] Y.A.K. Reddy, I.-k. Kang, Y.B. Shin, H.Ch Lee, P.S. Reddy, Mater. Sci. Semicond. Process. 32 (2015) 107–116.
[23] D. Pjević, T. Marinković, J. Savić, N. Bundaleski, M. Obradović, M. Milosavljević, M. Kulik, Thin Solid Films 591 (2015) 224–229.
[24] D. Pjević, M. Obradović, T. Marinković, A. Grce, M. Milosavljević, R. Grieseler, T. Kups, M. Wilke, P. Schaaf, Physica B: Condens. Matter 463 (2015) 20–25.
[25] Y.A. Kumar Reddy, Y.B. Shin, I.-K. Kang, H.C. Lee, Ceram. Int. 42 (2016) 17123–17127.
[26] Y.A. Kumar Reddy, Y.B. Shin, I.-K. Kang, H.C. Lee, P.S. Reddy, Appl. Phys. Lett. 107 (2015) 023503.
[27] G. Cacciato, F. Ruffino, M. Zimbone, R. Reitano, V. Privitera, M.G. Grimaldi, Mater. Sci. Semicond. Process. 42 (2016) 40–44.
[28] I. Manouchehri, K. Gholami, B. Astinchap, R. Mordian, D. Mehrparvar, Opt.-Int. J. Light Electron Opt. 127 (2016) 5383–5389.
[29] J.J. Huang, Ch.W. Kuo, W.Ch Chang, T.H. Hou, Appled Phys. Lett. 96 (2010) 262901.
[30] G.L. Chiarello, C. Tealdi, P. Mustarelli, E. Selli, Materials 9 (2016) 279.
[31] L.Y. Lin, Ch.P. Lee, R. vital, K. Ch Ho, J. Power Source 195 (2010) 4344–4349.
[32] R. Swanepoel, J. Phys. E: Sci. Instrum. 16 (1983) 1214–1223.
[33] Ch-Ch Ting, S.-Y. Chen, D.-M. Liu, J. Appl. Phys. 88 (2000) 4628–4633.
[34] L.V. Maneeshya, V.S. Anitha, P.V. Thomas, K. Joy, J. Mater. Sci.: Mater. Electron. 26 (5) (2015) 2947–2954.
[35] R.A. Smith, Semiconductors, 2nd edition, Cambridge University Press, Cambridge NY, 1978.
[36] J. Tauc, Mater. Res. Bull. 3 (1968) 37–46.
[37] F. Zhang, R.-J. Zhang, D.-X. Zhang, Z.-Y. Wang, J.-P. Xu, Y.-X. Zheng, L.-Y. Chen, R.-Z. Huang, Y. Sun, X. Chen, X.-J. Meng, N. Dai, Appl. Phys. Express 6 (2013) 121101–121104.
[38] F. Urbach, Phys. Rev. 92 (1953) 1324.
[39] N. Mott, E. Davis, Electronic Process in Non-Crystalline Materials, second ed, Clarendon Press, Oxford, UK, 1979.
[40] Salwan K. Al-Ani, Iraqi J. Appl. Phys. 4 (1) (2008) 17–23.
[41] M.M. Abd El-Raheem, Ateyyah M. Al-Baradi, Int. J. Phys. Sci. 8 (31) (2013) 1570–1580.
[42] S.H. Wemple, Phys. Rev. B. 7 (8) (1973) 3767–3777.
[43] S.H. Wemple, M. Didomenico Jr, Phys. Rev. B. 3 (1971) 1338–1351.
[44] E. Marquez, A.M. Bernal-Oliva, J.M. Gonzalez-Leal, R. Pricto-Alcon, A. Ledesma, R. Jimenez-Garay, I. Martil, Mater. Chem. Phys. 60 (3) (1999) 231–239.
[45] E. Marquez, P. Nagels, J.M. Gonzalez-Leal, A.M. Bernal Oliva, E. Sleeckx, R. Callaerts, Vacuum 52 (1999) 55–60.